PEGylated Gold Nanoparticles Conjugated to Monoclonal F19 Antibodies as Targeted Labeling Agents for Human Pancreatic Carcinoma Tissue

Wolfgang Eck,[†] Gary Craig,[‡] Aruna Sigdel,[‡] Gerd Ritter,[§] Lloyd J. Old,[§] Laura Tang,[∥] Murray F. Brennan,[¶] Peter J. Allen,[¶] and Michael D. Mason[‡,*]

[†]Applied Physical Chemistry, University of Heidelberg, Germany, and Institute for Molecular Biophysics, The Jackson Laboratory, Bar Harbor, Maine 04609, [‡]Department of Chemical and Biological Engineering and Institute for Molecular Biophysics, University of Maine, Orono, Maine 04469, [§]Ludwig Institute for Cancer Research,1275 York Avenue, New York, New York 10021, [∥]Department of Pathology, Memorial Sloan-Kettering Cancer Center, 1275 York Avenue, New York, New York 10065, and [¶]Department of Surgery, Memorial Sloan-Kettering Cancer Center, 1275 York Avenue, New York, New York 10065

ABSTRACT In this study, we describe optical detection of antibody-conjugated nanoparticles bound to surgically resected human pancreatic cancer tissue. Gold nanoparticles stabilized by heterobifunctional polyethylene glycol (PEG) were prepared using ~15 nm spherical gold cores and covalently coupled to F19 monoclonal antibodies. The heterobifunctional PEG ligands contain a dithiol group for stable anchoring onto the gold surface and a terminal carboxy group for coupling of antibodies to the outside of the PEG shell. The nanoparticle—antibody bioconjugates form highly stable dispersions and exhibit long-term resistance to agglomeration. This has been demonstrated by dynamic light scattering, size exclusion chromatography, and transmission electron microscopy. The nanoparticle bioconjugates were used to label tumor stroma in approximately 5 μm thick sections of resected human pancreatic adenocarcinoma. After rinsing away nonbound nanoparticles and fixation, the tissue samples were imaged by darkfield microscopy near the nanoparticle resonance scattering maximum (~560 nm). The images display pronounced tissue features and suggest that this novel labeling method could provide for facile identification of cancer tissue. Tumor samples treated with gold nanoparticles conjugated to nonspecific control antibodies and noncancerous pancreatic tissue treated with mAb-F19-conjugated gold nanoparticles both exhibited correctly negative results and showed no tissue staining.

KEYWORDS: targeted gold nanoparticles · heterobifunctional polyethylene glycol · F19 monoclonal antibody · pancreatic cancer · tissue labeling · darkfield microscopy

In recent years, improved imaging and analytical tools have led to new solution phase chemistries, providing effective size and geometry control over the growth of nanocrystals.[1] Metal nanoparticles are attracting strong interest in the fundamental sciences and are being widely investigated for their potential use in a range of technological and biological applications. For example, potential uses include subwavelength optical devices,[2] solar cells,[3] flexible electronics, conducting inks and adhesives,[4−6] surface-enhanced spectroscopies,[7] chemical catalysis,[8,9] and biological labeling and detection.[10,11]

Interest has recently developed into the use of metallic nanoparticles for the diagnosis and staging of cancer in humans. The accurate assessment of tumor stage is essential as local or systemic therapies are administered in a stage-specific fashion. Generally, oncologic therapies are categorized as either local (operative resection or radiation therapy) or systemic (chemotherapy with either cytotoxic or biologic agents). Patients who present with malignancy that is determined to be localized on pretreatment staging studies are typically treated with local therapy such as surgical resection or radiation. In the setting of metastatic disease, systemic treatment is generally recommended. With few exceptions, operative removal of the primary lesion has never been shown to improve survival when metastatic disease can be identified, and because of this, operative resection is generally avoided in patients with advanced malignancy. Improvements in imaging may allow for better diagnostics and thus allow physicians to better determine appropriateness of operative resection.

The current difficulties in the identification of metastatic disease are exemplified in patients with pancreatic adenocarcinoma. Patients who present with pancreatic adenocarcinoma often have small (<1 cm) metastatic deposits in the peritoneal cavity and/or liver that may not be identified on cross-sectional imaging studies (CT or MRI).[12−14] Laparoscopy is a minimally invasive optical inspection technique that has been utilized to identify small

*Address correspondence to michael.mason@maine.edu.

Received for review July 7, 2008 and accepted October 09, 2008.

Published online November 4, 2008.
10.1021/nn800429d CCC: $40.75

metastatic deposits not visualized on cross-sectional imaging.[15,16] Unfortunately, the effectiveness of laparoscopy relies on the ability of the surgeon to identify potential metastases based solely on tissue surface morphology and also only allows visual inspection of the organ surface. The uncertainty in this determination is evidenced by the fact that approximately 30% of patients who are thought to be without metastatic disease following laparoscopy, and who undergo surgical resection, die from metastatic disease within 7 months of operation.[17] Improved detection and assessment of small volume metastases may allow for the avoidance of operation in those with disease more appropriately treated with systemic therapy.

Due to their intense light scattering power, gold nanoparticles targeted to cancer tissue may improve the ability of surgeons to identify metastatic lesions either preoperatively or at the time of laparoscopy or histology during resection. Specifically, the tunability of their optimal scattering wavelength (plasmon resonance) may provide a means with which the apparent optical contrast of lesions, relative to neighboring tissue, can be dramatically enhanced. In addition, the properties of these particles make them detectable on routine forms of radiographic imaging (*e.g.*, X-ray-computed tomography).[18,19]

The light scattering signal from individual nanoparticles can be so strong that they can be viewed at video rates in live cells or thin tissue sections using conventional darkfield microscopy.[20,21] When imaged by scattering methods, metal nanoparticles may have several potential advantages over commercial stains or organic molecular or semiconductor quantum dot fluorophores.[7,22] Because photons are being scattered and not absorbed in these methods, these nanoprobes do not exhibit power-dependent excitation limitations such as photobleaching or intermittency, making it possible to image over extended periods of time. Their dimensions can be tuned for peak optical activity at longer wavelengths, allowing for the use of red NIR light sources capable of improved optical penetration into biological samples while simultaneously reducing background autofluorescence. Furthermore, when compared to semiconductor materials (*e.g.*, CdSe), or most organic dyes, noble metals are relatively nontoxic, making them well suited for *in vivo* studies.[23]

While these nanoparticles appear to show great promise, there still exist significant issues that must be overcome before they can be used effectively and quantitatively as probes in biological systems. A major goal in current nanoparticle research, and biolabeling in general, is the development of preparations that are long-circulating and can label-specific locations or biomarkers with high selectivity. Specifically, nanoparticles need to be stable in biological medium, for example, in tissue samples or in the bloodstream of living organisms, and show little or no biologically induced agglomeration or rapid clearance by components of the immune system. Ideally, targeted nanoparticles should recognize a biological receptor with high selectivity while demonstrating little nonspecific binding to other cellular components.

Commercial antibody-functionalized gold nanoparticles, now referred to as "immunogold", have been used for some time to label biological samples for imaging by electron microscopy.[8,24−27] Typical immunogold nanoparticle preparations involve the direct physisorption of antibodies to the surface of gold nanoparticles (<30 nm). The result is a system wherein at equilibrium both nanoparticle-bound and free (nonbound) antibody exists, diminishing the overall labeling efficiency. In addition, such nanoparticles usually exhibit poor biocompatibility or protein repellency and therefore tend to agglomerate *via* nonspecific, uncontrollable adsorption of proteins. Nonspecific labeling of undesired biological targets can be a further problem with antibody-functionalized, nonspecifically repellant surfaces, as we have shown in a previous study.[28]

Polyethylene glycol (PEG) bound to the surfaces of nanoparticles has been used for some time to render them resistant against protein adsorption, enhance their biocompatibility, and to stabilize them against agglomeration in biological environments.[29−39] PEGylated nanoparticles with diameters below 100 nm may become long-circulating in the bloodstream of live animals and have been called "stealth" particles since they can evade recognition by T cells and macrophages *in vivo* and thus avoid rapid clearance by the immune system.[37,40]

In a previous study using PEG thiol monolayers on planar gold surfaces, we have studied the antibody−antigen selectivity of polyclonal IgG antibodies immobilized on monolayers of heterobifunctional PEG monothiols (*i.e.*, PEG with two chemically different chain ends).[28] The antibodies were covalently attached to the outer ends of the PEG monolayers *via* amide bonds. The biological selectivity of these antibodies toward their respective antigens remained completely intact when they were embedded in a protein-repellent PEG matrix that suppresses nonspecific binding of other proteins. However, when the same antibody−antigen recognition experiments were performed on flat gold surfaces without any intermediate PEG layer, the biological selectivity of the immobilized antibodies was lost and nonspecific protein adsorption on the surface dominated. Immobilization of antibodies on the outside of heterobifunctional PEG coatings is therefore a highly suitable method when high selectivity of a biologically targeted surface is the desired goal.[28] Heterobifunctional PEG has been used before to prepare several varieties of bioconjugated nanoparticles conjugated to peptides, folic acid, or antibodies.[29,30,32−35,41,42] Two examples of mixed length PEG monolayers on gold nanoparticles containing both monofunctional and het-

erobifunctional PEG thiols have been reported very recently.[43,44] Antibodies were coupled to these two-component PEG shells *via* terminal carboxy or hydrazide groups. Other PEGylated gold nanoparticle−antibody conjugates have been described using a short heterobifunctional carbon linker molecule to attach the antibody directly to the gold surface and a long-chain mPEG monothiol to fill up the remaining spaces on the nanoparticle surface, partially covering the targeting antibody.[39] While these approaches represent significant improvements over previous synthetic strategies, the use of PEG linkers of short (<10 EG units) or mixed average length may reduce synthetic control and consistency between particles due to the expected statistical composition distribution of mixed PEG monolayers.

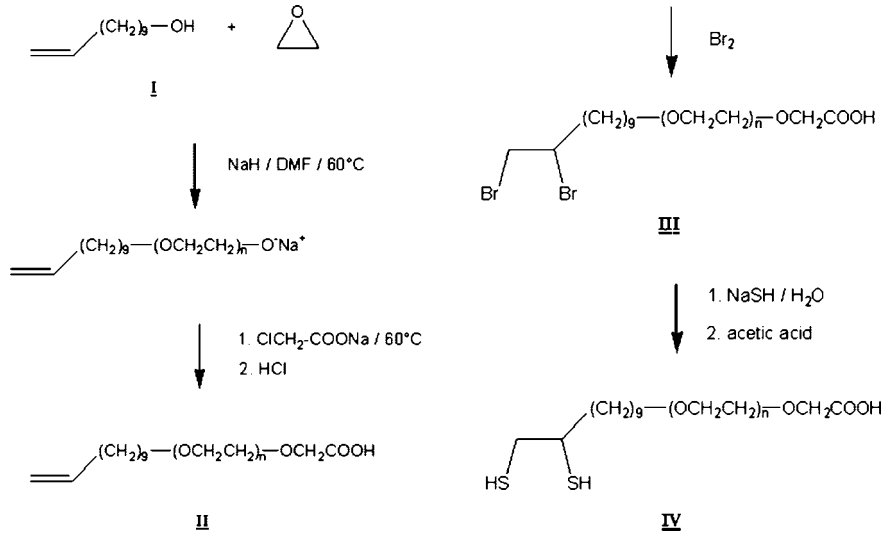

Figure 1. Synthesis scheme of the carboxy-terminated PEG dithiol (C-PEG-2S). The final product is shown as structure 4. Here $n_{av} = 25$ was used.

Dithiols such as dihydrolipoic acid derivatives, lipoic acid as the corresponding disulfide,[32,38,42,45] and di- or polythiol polyethylene glycols[43,46] have been used to functionalize gold nanoparticles, improving monolayer stability. Due to their multidentate nature, these species couple more rapidly and stably to many nanoparticle surfaces than comparable monothiols. Heterobifunctional PEG is commonly prepared by polymerization of ethylene oxide and sequential addition of the two different chain ends to the polymer.[28,47,48] Functionalization of commercially available homobifunctional polyethylene glycols by two different end groups as a means to prepare heterobifunctional PEG is problematic since statistical product mixtures of molecules with different end groups are obtained which can only be separated chromatographically at low molecular weights of the PEG chain.

In order to reproducibly obtain nanoparticle samples with high biological selectivity, in-depth characterization by physical methods such as dynamic light scattering, size exclusion chromatography, and electron microscopy is highly desirable in order to control factors such as particle size distribution, antibody content per particle, and stability against agglomeration. A general need for physicochemically well-defined gold nanoparticle−antibody conjugates to facilitate their application in biology or medicine is now widely recognized.[39]

We present here a novel heterobifunctional PEG coating for gold nanoparticles that is stably anchored on the gold surface *via* dithiol anchor groups on one end of the PEG chain and allows facile attachment of biological signal molecules *via* carboxy groups on the other outer end of the PEG ligand. A single PEG component with an average degree of polymerization of 25 EG units is used to form a nanoparticle shell that ensures consistently high selectivity and stability of the covalently bound targeting moieties. We further present the use of a novel probe system using a monoclonal antibody (mAb) with high specificity for tumor stroma (*i.e.*, the connective tissue surrounding the tumor). This humanized murine antibody is directed against fibroblast activation protein (FAP-α) which is a serine protease produced specifically by activated fibroblasts.[49−51] In phase I clinical trials, this antibody has been found to be safe and specific for FAP-α-producing tumor stroma.[52] To ensure long-term stability, the F19 antibody is covalently attached to the PEGylated nanoparticles *via* their exposed carboxyl end groups. The resulting antibody−nanoparticle conjugates are nearly agglomerate-free, are highly stable as single particles in buffer and in the presence of proteins, and retain the desired target specificity of the F19 antibody. This latter property is confirmed by comparing labeled and unlabeled pancreatic tissue sections using darkfield microscopy, taking advantage of the strong tunable scattering properties of the bioconjugate nanoparticle core as the image contrast mechanism.

RESULTS AND DISCUSSION

Synthesis and Characterization of Nanoparticle Conjugates. The as-synthesized C-PEG-2S ligand **4** (Figure 1) was analyzed by MALDI mass spectrometry and ^{1}H NMR. The MALDI mass spectrum in Figure 2A shows the typical chain length distribution of anionically polymerized PEG. No higher oligomers such as dimers or trimers are visible in the spectrum. By integration of the peaks, both the mass (M_w) and number (M_n) average molecular weights can be obtained from the spectrum, where $M_w = 1347$ g/mol and $M_n = 1301$ g/mol. From ^{1}H NMR, M_n can be determined by comparison of the signal in-

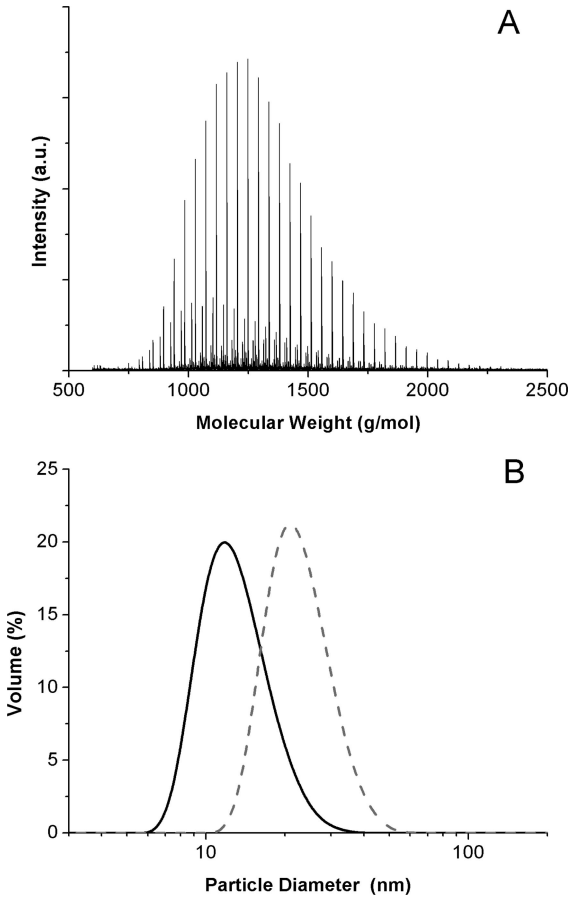

Figure 2. (A) MALDI mass spectrum of the as-prepared C-PEG-2S (**4**) showing its chain length distribution. By integration of the peaks, the weight and number average molecular weights and the polydispersity index can be calculated: M_w = 1347, M_n = 1301, M_w/M_n = 1.035. (B) Particle size distributions of gold nanoparticles with ~15 nm core diameter in water stabilized by citrate (solid line) and functionalized with the C-PEG-2S ligand (dashed gray line).

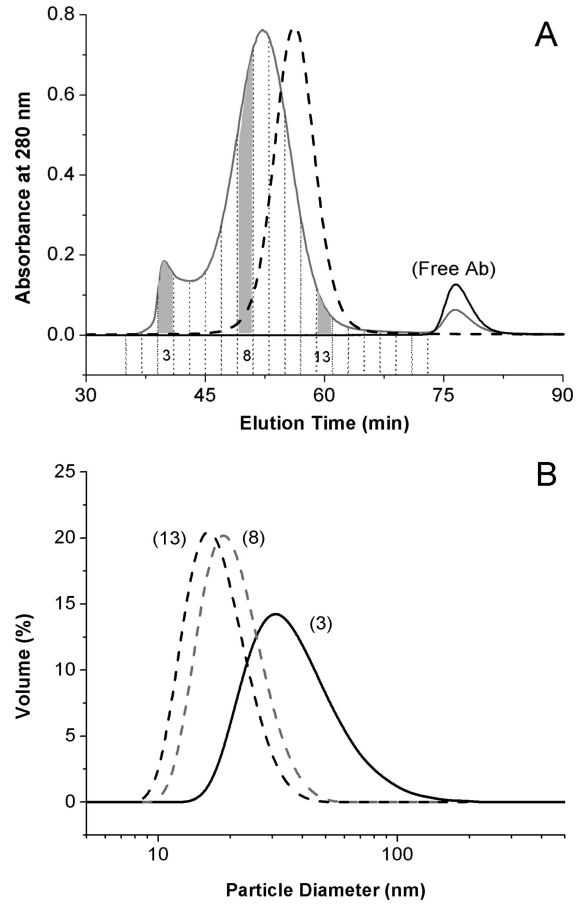

Figure 3. (A) Size exclusion chromatography elution profile of gold nanoparticles coated with the C-PEG-2S ligand before (dashed line) and after coupling of antibodies (solid gray line). Vertical dashed lines represent the 400 μL sampling fractions. Residual free antibody after coupling appears as the lower peak at 78 min (Free AB), as compared to the total initial antibody peak (black line). (B) Size distribution analysis of individual SEC fractions (3, 8, 13) from the as-prepared antibody-functionalized sample.

tensities of the polyether protons ($O-CH_2-CH_2-O$) and the protons of the terminal aliphatic carbon chain in **4**. M_n determined in this way is 1380 g/mol, which is consistent with the MALDI results. The conversion of the dibromide **3** to the dithiol **4** is not fully quantitative (45% yield according to ^1H NMR); however, the main product with a terminal dithiol group cannot be isolated easily by chromatography or by crystallization since the long PEG chain (n_{av} = 25) suppresses sufficient chemical differentiation between different end groups. For the final application as a surface ligand for gold nanoparticles, this may be of secondary importance since dithiols will chemisorb highly preferentially on gold nanoparticles.

The particle size distributions (calculated by volume), obtained from dynamic light scattering measurements, for the citrate-stabilized and C-PEG-2S surface-modified nanoparticles are shown in Figure 2B. As expected, the average hydrodynamic radius increases from the initial diameter of ~15 to ~25 nm (*z* average values) by the addition of the 25-mer C-PEG-2S ligand. The monomodal distribution suggests that the particles remain well dispersed as single entities and do not form agglomerates.

In Figure 3A, the SEC elution profiles of the gold nanoparticles coated with the C-PEG-2S ligand and exposed to the F19 antibody, obtained on a Superose 6 column, are shown with (gray line) and without (dashed line) preactivation of terminal carboxyl species with EDC/NHS. When properly activated, it is apparent that the size of the nanoparticles increases during antibody coupling, as shorter elution times correspond to larger particle diameters. Any remaining antibody that has not coupled to the NHS-activated particles appears as a separate peak at an elution time of ~78 min. When we used PEGylated gold nanoparticles that were not activated by NHS groups and treated with IgG under identical conditions, we observed no change in the elution profile, and all initially used antibody was recovered (free AB peak in Figure 3A). This suggests that chemically nonactivated gold nanoparticles covered with C-PEG-2S do not physisorb the antibody onto their surface. After prolonged storage of the GNP-F19 conju-

gates in a refrigerator for several months at 4 °C, we were not able to detect any free antibody by SEC, which indicates high stability and shelf life of the particle−antibody conjugates.

The particle size distributions obtained from light scattering are shown in Figure 3B for three of the 400 μL SEC fractions. The SEC fractions eluted first contain particle conjugates with the largest hydrodynamic diameters, ranging up to more than 100 nm in SEC fraction 3, which contained all particles larger than the exclusion limit (*i.e.*, the pore size) of the SEC column material, which is about 40−45 nm for Superose 6.

TEM images of the SEC fractions, shown in Figure 4, agree with the light scattering data. Here the fractions eluted first contain larger cross-linked aggregates (Figure 4A). The regularly appearing gaps between different gold nanoparticles, shown in the inset of Figure 4A, most likely contain organic material that is not displayed by TEM. Since the coupling of antibody to the NHS-activated gold nanoparticles proceeds in a random fashion *via* any free amino groups present on an IgG molecule, stemming mainly from lysine residues, an antibody molecule can react with more than one nanoparticle and thus cross-link them. We found that the amount of large, cross-linked material isolated in the earlier SEC fractions tends to decrease with a higher volume of the reaction mixture containing the activated particles and the antibodies since hydrolysis of the activated NHS esters always competes with the coupling reaction. The particles eluted in the middle and later fractions (*e.g.*, fraction 8), shown in Figure 4B, contain mostly individual GNP−F19 conjugates. These particle−antibody conjugates are completely stable and do not agglomerate. As a control, we verified the actual presence of the antibody in SEC fractions 3, 8, and 13 by release of the PEG ligand from the nanoparticles by treatment with mercaptoethanol and subsequent analysis of the antibody fragments obtained on an SDS page gel (see below). In order to ensure antibody binding and minimize the application of aggregates, fractions 7−10 were used for tissue labeling.

Quantitative determination of the amount of antibody in a single SEC fraction turned out to be more problematic than anticipated. Since gold nanoparticles have a rather strong light absorption through most of the visible and the UV range, they provide an enormously high background when standard colorimetric protein determination methods are used. Even in the micro-bicinchoninic acid (BCA) assay, one of the most sensitive colorimetric protein assays available,[53] the light absorption of the gold nanoparticles themselves turned out to be about an order of magnitude larger than the light absorption generated by the protein assay. As a consequence, the gold particles have to be separated from the protein assay before the measurement. One way to overcome this effect is to chemically separate the antibodies from the gold particle followed by analysis of the stripped protein. However, when the PEG ligand is removed from the particles together with the covalently bound antibodies, the gold particles are destabilized and lose their protein resistance, which leads to adsorption of the protein on the bare gold surface, partial removal of antibody from the analyte solution, and thus to false results.

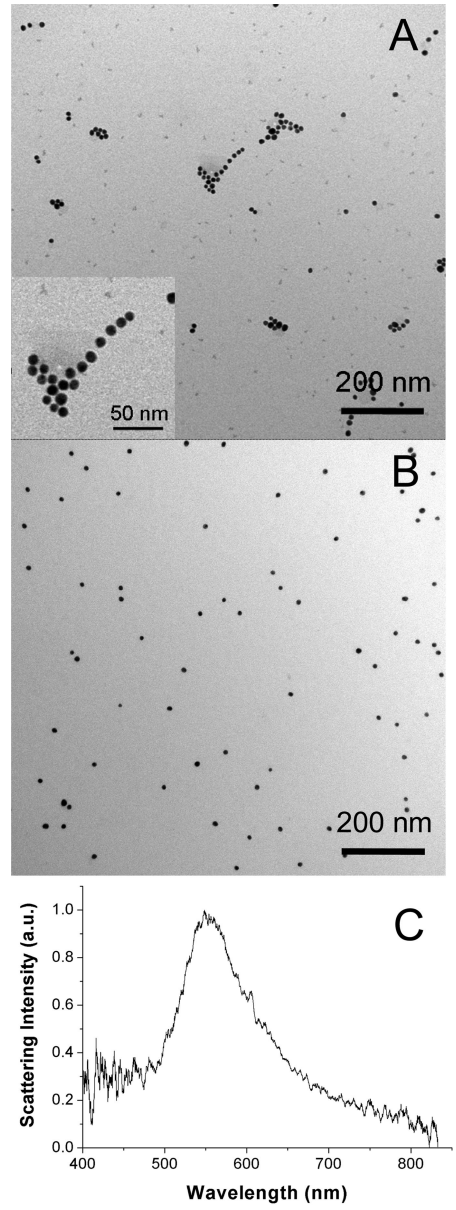

Figure 4. Transmission electron microscopy images of SEC fractions 3 and 8 (A and B, respectively) of GNP−F19. Aggregates are clearly visible in fraction 3, whereas predominantly individual nanoparticles are present in fraction 8. An expanded image of gold nanoparticle aggregates from SEC fraction 3 is also shown in A. (C) Darkfield scattering spectrum (light collected in the forward direction) for a collection of GNP−F19 conjugates dispersed on glass. The peak scattering wavelength is approximately 560 nm.

We also conducted a micro-BCA assay using the original gold−PEG−antibody conjugates, so that the bicinchoninic acid copper complex generated could diffuse away from the particles and dissolve in the sur-

rounding aqueous solution. However, after removal of the gold nanoparticle−PEG−antibody conjugates by centrifugation, the amount of antibody measured was too high by factors of about 10−50. This is consistent with a previously reported result[39] and may be caused by the sensitivity of the BCA assay toward thiols, which are present here as the anchor groups of the C-PEG-2S ligand on the gold particle surface.

We also attempted determination of the bound antibody by releasing the PEG ligand together with the antibody from the particles by treatment with mercaptoethanol and subsequent protein quantification on an SDS-PAGE gel (staining with SYPRO-Ruby). However, we observed intense smearing of the protein bands on the gel, most likely caused by nonspecific adsorption of the antibody on the bare, non-PEGylated particles.

Other simple optical methods such as fluorescence similarly cannot be used to quantify the amount of bound antibody since the strong electrical field in the vicinity of the particle surface alters or quenches electronic transitions of attached chromophores even at distances of more than 10 nm from the surface.[54,55] When we attached antibodies labeled with fluorescein to the gold particles, the fluorescence of the samples purified by SEC was partially retained and could be measured; however, after subtraction of the background caused by the gold particles themselves, the fluorescence yield was consistently lower than that calculated from the amount of antibody in the sample determined by SEC.

The average amount of covalently attached antibody per nanoparticle could be determined from the difference between the total original amount of antibody used and the amount of free antibody recovered during size exclusion chromatography (free AB peaks in Figure 3A). The area of the peak at 78 min was calibrated with a known amount of mAb-F19 which was quantified by its light absorption at 280 nm. The total mass of gold present in a given sample was determined using the light absorption of the sample at the absorption maximum of gold nanoparticles (Figure 4C). After the average radius of the gold particles has been determined by dynamic light scattering and confirmed by electron microscopy, the number of gold nanoparticles in a sample and the average number of IgG molecules per particle was calculated. By this method, we estimate that typical average loading values in a given gold nanoparticle sample are between 4 and 6 antibodies per particle. Note that this method can only determine the average amount of antibody in an entire nanoparticle sample, not in an individual SEC fraction.

Pancreatic Tissue Labeling. Since the PEGylated gold nanoparticle−antibody conjugates are highly stable as single particles and do not easily agglomerate in the presence of protein, they can be effectively used for staining of biological samples. As a demonstration of their labeling potential, we chose human pancreatic cancer tissue, whose stroma (*i.e.*, the connective tissue surrounding the tumor) is known to react with the F19 monoclonal antibody. The F19 antigen is a cell surface glycoprotein (fibroblast activation protein, FAP-α) that is highly expressed by the stromal tissue of various cancer types such as breast, lung, colon, pancreas, head, and neck cancer.[56,57]

This stromal-specific approach is particularly applicable to pancreatic cancer because of its almost unique ability to elicit an extreme fibrotic response. Immunohistochemical staining performed with F19 mAb of *ex vivo* human pancreatic cancer specimens has demonstrated consistent intense staining of tumor stroma,[51,56] which is nearly absent in adjacent normal tissue. The amount of staining observed can vary with different tumors depending on the level of FAP-α expression. We have observed this fibrotic response uniformly in both primary pancreatic tumors as well as in biopsy specimens of small (<5 mm) liver metastases (data not shown).

Gold nanoparticles with diameters between 12 and 20 nm are known to efficiently scatter visible light in the wavelength region around 530 nm and can thus easily be detected by wavelength selection using optical methods such as darkfield or confocal microscopy.[58] In order to determine the optimal scattering wavelength to be used for tissue imaging, absorption spectra for the GNP−F19 dispersion and darkfield scattering spectra for individual GNP−F19 conjugates dispersed on glass were obtained as shown in Figure 4C. As predicted by Rayleigh scattering for a distribution of gold nanoparticles in this size range, a small shift in the absorption and scattering maxima is observed. The maximum total optical attenuation, and subsequent image contrast in the darkfield transmission microscope used for tissue imaging, is expected to occur at the peak overlap between the absorption and scattering curves (~560 nm). As such, a 550 ± 20 nm dichroic band-pass filter was selected for imaging of the nanoparticle conjugates on tissue.

Optical measurements of labeled tissue are shown in Figure 5. There was found to be no significant difference in tissue labeling as a function of incubation time, so images presented are that of tissue incubated for 6 h. For comparison, an image area of a section of cancer tissue labeled by conventional immunohistochemical (IHC) secondary antibody staining of FAP-α is shown (Figure 5A). The presence of cancer stroma is indicated by the striated structures in red. The darkfield scattering image of GNP−F19-labeled cancer tissue (Figure 5B) exhibits the same apparent underlying stromal structure as that indicated by IHC staining, whereas the cancer control sample labeled with gold nanoparticles conjugated to nonspecific IgG antibody (Figure 5C), and the healthy tissue labeled with the GNP−F19 (Figure 5D) demonstrate minimal image contrast with only a few individual nanoparticles (small green spots) visible. For

the large image areas shown in Figure 5B−D, the presence of individual nanoparticles is not immediately obvious. Upon closer inspection, however, individual image features with dimensions consistent with the Abbe criteria for optical diffraction (~250 nm for 560 nm photons) are visible as shown in the inset in Figure 5B. Furthermore, the fact that the scattering wavelength of visible features remains unshifted relative to the 560 nm peak determined for individual GNP−F19 conjugates suggests that the tissue-bound particles remain optically isolated from one another. This does, however, not eliminate the possibility of aggregation.

It should, however, be noted that the observed image contrast can vary between cancer tissue sections labeled with GNP−F19 and different image locations within each section. This arises from normal molecular and structural variations in pancreatic cancer tissue, as immunohistochemical stainings with the F19 antibody and a secondary dye-labeled antibody show similar variability. In contrast, gold nanoparticles coupled to nonspecific control IgG or healthy tissue consistently showed no feature enhancement. In future work, we will investigate different cancer types and antibodies that may have increased potential for larger and more spatially homogeneous labeling yields.

CONCLUSIONS

Several previous studies used gold nanoparticles to label cancer cells grown in culture,[20,31,36,59−61] and in other studies, cells embedded in phantom tissue were similarly labeled.[62−64] A very recent study used antibody-labeled gold nanoparticles bearing Raman tags for tumor targeting in live mice and imaging by surface-enhanced Raman scattering.[44] To our knowledge, the study presented here is the first that uses antibodies covalently attached to PEGylated gold nanoparticles to label human cancer tissue that has been surgically resected from patients. We take advantage of the strong optical scattering properties of gold nanoparticles to image the actual spatial distribution of a tumor and its stromal tissue with a simple darkfield microscope. Since the gold nanoparticle−antibody conjugates are effectively stabilized by heterobifunctional PEG, they are highly stable under the biologically complex conditions of human tissue and unbound nanoparticles can be rinsed away almost quantitatively when the tissue does not contain the targeted antigen.

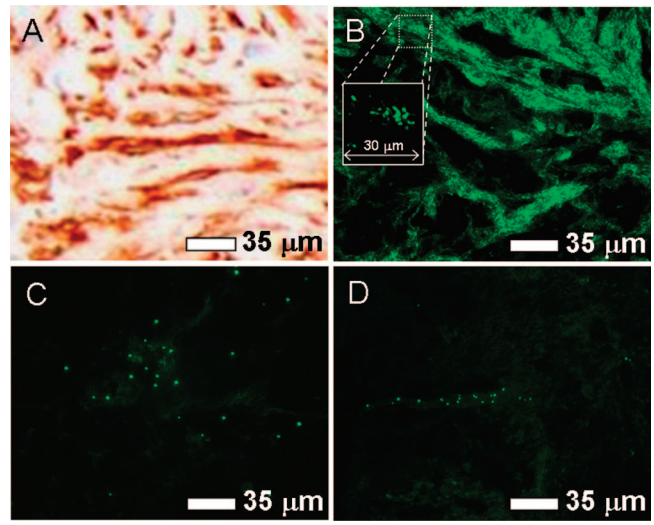

Figure 5. (A) Representative pancreatic cancer tissue thin sections labeled using secondary antibody staining (red regions). (B) Darkfield transmission scattering images of GNP−F19-labeled pancreatic cancer tissue, (C) GNP−F19-labeled healthy tissue, and (D) GNP−mIgG-labeled pancreatic cancer tissue. The expanded section in B has been contrast enhanced to emphasize the presence of individual GNP−F19.

While the general labeling efficiency of the GNP−F19 for any type of pancreatic tumor is as yet undetermined, the darkfield optical contrast, as evidenced by the images presented here, proved to be sufficiently bright for visualization of even individual particles or their aggregates by eye and could be imaged routinely under only 10× (low NA) magnification. This intense signal demonstrates the potential of this labeling technique for a number of clinical and surgical applications. However, since the scattering intensity depends on the sixth power of the particle diameter, according to Rayleigh scattering theory, larger gold nanoparticles are expected to produce an even stronger signal. The use of darkfield microscopy (transmission) presented here mandated the use of thin specimens. Since tissue is largely transparent in the near-infrared region of the electromagnetic spectrum, thicker samples may be examined when antibody-conjugated gold nanorods with a scattering maximum in the near-infrared are used.[20,33,39,62] Alternative microscopic methods such as widefield and confocal reflectance measurements, which are currently being conducted in our laboratory, may also allow for the investigation of thicker specimens and potentially *in vivo* (laparoscopic) imaging.

METHODS

Materials. All chemicals, buffers, and solvents were purchased from commercial sources and used as received. Monoclonal F19 IgG was received from the Ludwig Institute, New York, NY, as a solution in PBS stabilized with sodium azide. Nonspecific mouse IgG (ChromPure) was purchased from Jackson ImmunoResearch and used as received.

Synthesis of the PEG Ligand 4 (C-PEG-2S). The synthesis scheme of the carboxy-terminated PEG dithiol **4** (C-PEG-2S, n_{av} = 25) is shown in Figure 1. Compound **2** was synthesized by anionic polymerization of a 25-fold molar excess of ethylene oxide onto **1**.[28] Dibromide **3** was obtained by treatment of **2** with a 1.2-fold molar excess of elemental bromine in dichloromethane at 0 °C for 4 h in the dark. **3** was isolated by removal of the solvent using a slight vacuum and a water bath temperature of 30 °C in a rotary evaporator and final drying of the product in vacuum. **4** was obtained by dissolving **3** in water and subsequent reaction with a 10-fold molar excess of sodium hydrosulfide hydrate for 3

days at room temperature under nitrogen. Excess sodium hydrosulfide was destroyed by slow addition of excess acetic acid at 0 °C, and the resulting mixture was extracted five times with chloroform. The organic phase was dried with sodium sulfate, filtered, and the solvent was removed in vacuum in a rotary evaporator using a water bath temperature of 30 °C. The product was dissolved in ethanol at room temperature, recrystallized three times at −20 °C, and finally dried in vacuum.

The carboxy-terminated PEG dithiol **4** was analyzed by MALDI mass spectrometry (see Figure 2A) and ^{1}H NMR. MALDI mass spectrometry was performed on a Bruker Biflex using α-cyano-4-hydroxycinnamic acid as the matrix material. ^{1}H NMR spectra were taken on a Gemini 300 MHz device in perdeuterated dimethyl sulfoxide. ^{1}H NMR (300 MHz, DMSO-d_6): δ = 1.17−1.55 (m, 17H, CH_2, SH), 1.93−2.10 (br, 1H, SH), 2.75−2.83 (m, 3H, S−CH_2−CH−S), 3.35 (t, 2H, CH_2−CH_2−O, J = 7 Hz), 3.44−3.80 (m, 100H, OCH_2), 4.01 (s, 2H, CH_2−COOH), 12.20 (br, 1H, COOH).

Preparation of Gold Nanoparticle−Antibody Conjugates. Gold nanoparticles stabilized by citrate were prepared from hydrogen tetrachloroaurate in boiling water by reduction with sodium citrate as described previously.[53] In order to obtain a particle diameter of about 15 nm, 50 mg of $HAuCl_4 \times 3\ H_2O$ in 150 mL of water was used, and 132 mg of sodium citrate dissolved in 15 mL of water was added to the boiling solution.

Gold nanoparticles coated with the C-PEG-2S ligand were prepared from the citrate-stabilized gold nanoparticles by simple ligand exchange. Since gold nanoparticles stabilized by citrate agglomerate immediately upon transfer into salt containing buffer, the ligand exchange from citrate to PEG must be performed in pure water. Five hundred microliters of the as prepared citrate stabilized gold nanoparticle dispersion was added to 2 mg of the dry C-PEG-2S ligand and mixed well. Treatment of gold/citrate particles with this concentration of the PEG ligand in water leads to rapid coating with the PEG dithiol, and after several minutes, an increase of the hydrodynamic radius was measured by dynamic light scattering. The mixture was allowed to sit for ~2 h at room temperature. At this point, the nanoparticle dispersion was transferred into a 1.5 mL Eppendorf tube and centrifuged at 16 000*g* for 30 min, until a pellet was formed. The supernatant was removed, and 1 mL of 18 MΩ water was added. This process was repeated three times to remove any unreacted PEG ligand.

After final washing and decanting, the particles were resuspended into 100 μL of salt containing medium (0.1 M MES buffer, pH = 5), after which their size distribution remained completely stable (>1 year under exclusion of air and storage in a dark refrigerator), allowing for later functionalization with antibodies. The absence of free C-PEG-2S ligand in solution was confirmed by size exclusion chromatography using a refractive index detector, and the particle size, compared to the citrate stabilized particles, was determined by dynamic light scattering.

Attachment of antibodies to the PEGylated nanoparticles was performed using standard *N*-hydroxysuccinimide/1-ethyl-3-(3-dimethylaminopropyl)carbodiimide (NHS/EDC) coupling chemistry.[65,66] In this method, the carboxy groups on the particle surface are first activated by reaction with EDC hydrochloride and NHS in 0.1 M MES buffer (pH 5). Ten milligrams of NHS and 10 mg of EDC were first dissolved into 100 μL of MES buffer. Twenty-five microliters of this solution was added to 100 μL of the PEGylated particle dispersion and allowed to sit for 30 min at room temperature. Excess activation agents were removed by repeated washing (four times) with 300 μL of MES (pH = 5) at 0 °C in centrifuge filters (Millipore Ultrafree 0.5, 30 kDa cutoff), spinning down at 11 500*g* to no more than 25 μL each time.

Antibody attachment was performed by adding the concentrated activated nanoparticles to a dilute solution containing the antibody. First, 15 μg (~100 pmol) of the antibody (F19 or mouse IgG) was diluted to a volume of 300 μL with cold PBS buffer (0 °C) at pH 7.4. (If the antibody solution contains sodium azide as a preservative, as is typical for many IgGs, it must first be removed by repeated washing with cold PBS buffer in centrifuge filters, as it competes for the activated carboxy groups on the particles.) This solution was added to the centrifuge filter containing the 25 μL solution of activated gold particles and mixed well. The mixture was then spun down to 25 μL and rinsed once more with 300 μL of PBS (all at 0 °C). Finally, enough PBS buffer to obtain a final volume of 25−50 μL was added. The solution was mixed well and transferred into an Eppendorf tube and shaken gently overnight at room temperature. After this time, all NHS-activated carboxy groups have reacted or been hydrolyzed, so no additional quenching was necessary.

The gold nanoparticle−F19 and nonspecific murine IgG conjugates (GNP−F19 and GNP−mIgG) were fractionated and analyzed by size exclusion chromatography (SEC) using a Waters 650E chromatography system with a 10 mm × 100 mm Superose 6 column (GE Healthcare Life Sciences), followed by a Waters model 440 280 nm detector. The mobile phase was phosphate buffered saline (0.05 M sodium phosphate, 0.15 M NaCl, pH 7.0, 0.02% sodium azide) at a flow rate of 0.2 mL/min. Data were collected and analyzed using a Beckman 406 A/D converter and a Beckman System Gold system. The SEC eluates were fractionated into 400 μL aliquots that were further analyzed by dynamic light scattering, darkfield scattering spectroscopy,[21] and TEM.

Dynamic light scattering was performed with a Malvern Zetasizer Nano ZS using a 45 μL quartz cell either in water or in standard 1× PBS buffer with 1.02 cP as the viscosity and 1.335 as the refractive index of PBS at 25 °C. Transmission electron microscopy was done on a JEOL JEM-1230 device at 80 kV. Samples were prepared by dilution of the nanoparticles in water, placement of a drop (2−3 μL) on a copper grid carrying a 20 nm thick carbon film (CF-300-Cu, Electron Microscopy Sciences), and drying overnight.

Treatment of Pancreatic Cancer Tissue with Nanoparticle−Antibody Conjugates. Tissue samples were obtained of both cancerous and healthy human pancreas from patients undergoing pancreatic resection. Tissue sections were prepared by microtome to thicknesses of approximately 5 μm. These sections were fixed on glass slides using cold acetone (0 °C) for 10 min. After washing in PBS, the sections were incubated individually in a 1:10 dilution of the nanoparticle conjugates, GNP−F19, and GNP−mIgG (~50 μg/mL of bioconjugate to PBS buffer), for 3, 6, and 12 h. After incubation, the labeled samples were rinsed in PBS buffer multiple times to remove any unbound nanoparticle conjugate. The samples were then dried with a stream of N_2 and sealed under cover glass by standard methods. Control samples were similarly prepared using tissue sections of healthy pancreas labeled with GNP−F19 and cancer tissue labeled with a nonspecific mouse IgG monoclonal antibody. The resulting samples were imaged by darkfield microscopy, with wavelength selection near the GNP−F19 resonance scattering maximum using a dichroic filter (550 ± 20 nm), onto a digital camera (Moticam 1280 × 1024 pixels).

Acknowledgment. This work was supported in part by the Bildner fund, Memorial Sloan-Kettering Cancer Center, New York, NY, and the National Science Foundation/EPSCoR under Grant No. 0132384. The authors thank Robert Wilpan for performing the SEC experiments, Pete Finger for the TEM images, and Barbara Knowles and Michael Grunze of the Institute of Molecular Biophysics for continuing support.

REFERENCES AND NOTES

1. Alivisatos, P. A.; Gu, W.; Larabell, C. Quantum Dots as Cellular Probes. *Annu. Rev. Biomed. Eng.* **2005**, *7*, 55–76.
2. Shiraishi, Y.; Maeda, K.; Yoshikawa, H.; Xu, J.; Toshima, N.; Kobayashi, S. Frequency Modulation Response of a Liquid-Crystal Electro-Optic Device Doped with Nanoparticles. *Appl. Phys. Lett.* **2002**, *81*, 2845–2847.
3. Law, M.; Greene, L. E.; Johnson, J. C.; Saykally, R.; Yang, P. Nanowire Dye-Sensitized Solar Cells. *Nat. Mater.* **2005**, *4*, 455–459.
4. Fuller, S. B.; Wilhelm, E. J.; Jacobson, J. M. Ink-Jet Printed Nanoparticle Microelectromechanical Systems. *J. Microelectromech. Syst.* **2002**, *11*, 54–60.
5. Carotenuto, G.; Pepe, G. P.; Nicolais, L. Preparation and Characterization of Nano-Sized Ag/PVP Composites for Optical Applications. *Eur. Phys. J. B* **2000**, *16*, 11–17.
6. Lo, C. T.; Chou, K. S.; Chin, W. K. Effects of Mixing Procedures on the Volume Fraction of Silver Particles in

Conductive Adhesives. *Adhes. Sci. Technol.* **2001**, *15*, 783–792.
7. Mulvaney, S. P.; Musick, M. D.; Kearting, C. D.; Natan, M. J. Glass-Coated, Analyte-Tagged Nanoparticles: A New Tagging System Based on Detection with Surface-Enhanced Raman Scattering. *Langmuir* **2003**, *19*, 4784–4790.
8. Hughes, D. Immunogold Probes in Light Microscopy. In *Methods in Molecular Biology*; Burns, R., Ed.; Humana Press: Totowa, NJ, 2005; pp 173−192.
9. Pradhan, N.; Pal, A.; Pal, T. Silver Nanoparticle Catalyzed Reduction of Aromatic Nitro Compounds. *Colloids Surf., A* **2002**, *196*, 247–257.
10. Maxwell, D. J.; Taylor, J. R.; Nie, S. Self-Assembled Nanoparticle Probes for Recognition and Detection of Biomolecules. *J. Am. Chem. Soc.* **2002**, *124*, 9606–9612.
11. Salata, O. Applications of Nanoparticles in Biology and Medicine. *J. Nanobiotechnol.* **2004**, *2*, 3–8.
12. Tamm, E. P.; Lover, E. M.; Faria, S. C.; Evans, D. B.; Wolff, R. A.; Charnsangavej, C. Retrospective Analysis of Dual-Phase MDCT and Follow-up EUS/EUS-FNA in the Diagnosis of Pancreatic Cancer. *Abdom. Imaging* **2007**, *32*, 660–667.
13. Kulig, J.; Popiela, T.; Zajac, A.; Klek, S.; Kolodziejczyk, P. The Value of Imaging Techniques in the Staging of Pancreatic Cancer. *Surg. Endoc.* **2005**, *19*, 361–365.
14. White, R.; Winston, C.; Gonen, M.; D'Angelica, M.; Jarnagin, W.; Conlon, K.; Fong, Y.; Brennan, M.; Allen, P. Current Utility of Staging Laparoscopy for Pancreatic and Peripancreatic Neoplasms. *J. Am. Coll. Surgeons* **2007**, *9*, 445–450.
15. Conlon, K. C.; Dougherty, E.; Klimstra, D. S.; Coit, D. G.; Turnbull, A. D.; Brennan, M. F. The Value of Minimal Access Surgery in the Staging of Patients with Potentially Resectable Peripancreatic Malignancy. *Ann. Surg.* **1996**, *223*, 134–140.
16. Camacho, D.; Reichenbach, D.; Duerr, G. D.; Venema, T. L.; Sweeney, J. F.; Fisher, W. E. Value of Laparoscopy in the Staging of Pancreatic Cancer. *J. Pancreas* **2005**, *6*, 552–561.
17. Ferrone, C. R.; Haas, B.; Tang, L.; Coit, D. G.; Fong, Y.; Brennan, M. F.; Allen, P. J. The Influence of Positive Peritoneal Cytology on Survival in Patients with Pancreatic Adenocarcinoma. *J. Gastrointest. Surg.* **2006**, *10*, 1347–1353.
18. Hainfeld, J. F. S.; D. N.; Focella, T. M.; Smilowitz, H. M. Gold Nanoparticles: A New X-Ray Contrast Agent. *Br. J. Radiol.* **2006**, *79*, 248–253.
19. Kim, D. P.; S.; Lee, J. H.; Jeong, Y. Y.; Jon, S. Antibiofouling Polymer-Coated Gold Nanoparticles as a Contrast Agent for *in Vivo* X-Ray Computed Tomography Imaging. *J. Am. Chem. Soc.* **2007**, *129*, 7661–7665.
20. El-Sayed, I. H.; Huang, X.; El-Sayed, M. A. Surface Plasmon Resonance Scattering and Absorption of Anti-EGFR Antibody Conjugated Gold Nanoparticles in Cancer Diagnostics: Applications in Oral Cancer. *Nano Lett.* **2005**, *5*, 829–834.
21. Curry, A.; Hwang, W. L.; Wax, A. Epi-Illumination through the Microscope Objective Applied to Darkfield Imaging and Microspectroscopy of Nanoparticle Interaction with Cells in Culture. *Opt. Express* **2006**, *14*, 6535–6542.
22. Zheng, J.; Zhang, C.; Dickson, R., M. Higly Fluorescent, Water-Soluble, Size- Tunable Gold Quantum Dots. *Phys. Rev. Lett.* **2004**, *93*, 077402-1–077402-4.
23. Kirchner, C.; Liedl, T.; Kudera, S.; Pellegrino, T.; Javier, A. M.; Gaub, H. R.; Stoelzle, S.; Fertig, N.; Parak, W. J. Cytotoxicity of Colloidal CdSe and CdSe/ZnS Nanoparticles. *Nano Lett.* **2005**, *5*, 331–338.
24. Hermann, R.; Walther, P.; Mueller, M. Immunogold Labeling in Scanning Electron Microscopy. *Histochem. Cell Biol.* **1996**, *106*, 31–39.
25. Wooding, F. B. P.; Kendall, M. D. Immunogold Methods for Electron Microscopy. *Methods. Immunol. Anal.* **1993**, *3*, 314–337.
26. Verkleij, A. J.; Koster, A. J.; Muller, W. H.; Humbel, B. M. Immuno-Gold Labeling in Transmission Electron Microscopy. *NATO ASI Ser. A, Life Sci.* **1999**, *309*, 339–356.
27. Hainfeld, J. F.; Powell, R. D. New Frontiers in Gold Labeling. *J. Histochem. Cytochem.* **2000**, *48*, 471–480.
28. Herrwerth, S.; Rosendahl, T.; Feng, C.; Fick, J.; Eck, W.; Himmelhaus, M.; Dahint, R.; Grunze, M. Covalent Coupling of Antibodies to Self-Assembled Monolayers Of Carboxy-Functionalized Poly(Ethylene Glycol): Protein Resistance and Specific Binding of Biomolecules. *Langmuir* **2003**, *19*, 1880–1897.
29. Otsuka, H.; Akiyama, Y.; Nagasaki, Y.; Kataoka, K. Quantitative and Reversible Lectin-Induced Association of Gold Nanoparticles Modified with α-Lactosyl-ω-Mercapto-Poly(Ethylene Glycol). *J. Am. Chem. Soc.* **2001**, *123*, 8226–8230.
30. Otsuka, H.; Nagasaki, Y.; Kataoka, K. PEGylated Nanoparticles for Biological and Pharmaceutical Applications. *Adv. Drug Delivery Rev.* **2003**, *55*, 403–419.
31. Kim, J.; Park, S.; Lee, J. E.; Jin, S. M.; Lee, J. H.; Lee, I. S.; Yang, I.; Kim, J.; Kim, S. K.; Cho, M.; et al. Designed Fabrication of Multifunctional Magnetic Gold Nanoshells and Their Application to Magnetic Resonance Imaging and Photothermal Therapy. *Angew. Chem., Int. Ed.* **2006**, *45*, 7754–7758.
32. Garcia, B.; Salome, M.; Lemelle, L.; Bridot, J.-L.; Gillet, P.; Perriat, P.; Roux, S.; Tillement, O. Sulfur K-Edge XANES Study of Dihydrolipoic Acid Capped Gold Nanoparticles: Dihydrolipoic Acid is Bound by Both Sulfur Ends. *Chem. Commun.* **2005**, 369–371.
33. Pierrat, S.; Zins, I.; Breivogel, A.; Soennichsen, C. Self-Assembly of Small Gold Colloids with Functionalized Gold Nanorods. *Nano Lett.* **2007**, *7*, 259–263.
34. Shenoy, D.; Fu, W.; Li, J.; Crasto, C.; Jones, G.; DiMarzio, C.; Sridhar, S.; Amiji, M. Surface Functionalization of Gold Nanoparticles Using Hetero-Bifunctional Poly(Ethylene Glycol) Spacer for Intracellular Tracking and Delivery. *Int. J. Nanomedicine* **2006**, *1*, 51–57.
35. Sperling, R. A.; Pellegrino, T.; Li, J. K.; Chang, W. H.; Parak, W. J. Electrophoretic Separation of Nanoparticles with a Discrete Number of Functional Groups. *Adv. Funct. Mater.* **2006**, *16*, 943–948.
36. Liu, Y.; Shipton, M. K.; Ryan, J.; Kaufman, E. D.; Franzen, S.; Feldheim, D. L. Synthesis, Stability, and Cellular Internalization of Gold Nanoparticles Containing Mixed Peptide-Poly(Ethylene Glycol) Monolayers. *Anal. Chem.* **2007**, *79*, 2221–2229.
37. Gref, R.; Couvreur, P. Stealth and Biomimetic Core-Corona Nanoparticles. In *Encyclopedia of Nanoscience and Nanotechnology*; Nalwa, H. S., Ed.; American Scientific Publishers: Stevenson Ranch, CA, 2004; pp 83−94.
38. Dixit, V.; Van den Bossche, J.; Sherman, D. M.; Thompson, D. H.; Andres, R. P. Synthesis and Grafting of Thioctic Acid-PEG-Folate Conjugates onto Au Nanoparticles for Selective Targeting of Folate Receptor-Positive Tumor Cells. *Bioconjugate Chem.* **2006**, *17*, 603–609.
39. Liao, H.; Hafner, J. H. Gold Nanorod Bioconjugates. *Chem. Mater.* **2005**, *17*, 4636–4641.
40. Owens, D. E.; Peppas, N. A. Opsonization, Biodistribution, and Pharmacokinetics of Polymeric Nanoparticles. *Int. J. Pharm.* **2006**, *307*, 93–102.
41. Sun, C.; Sze, R.; Zhang, M. Folic Acid-PEG Conjugated Superparamagnetic Nanoparticles for Targeted Cellular Uptake and Detection by MRI. *J. Biomed. Mater. Res., Part A* **2006**, *78A*, 550–557.
42. Abad, J. M.; Mertens, S. F. L.; Pita, M.; Fernandez, V. M.; Schiffrin, D. J. Functionalization of Thioctic Acid-Capped Gold Nanoparticles for Specific Immobilization of Histidine-Tagged Proteins. *J. Am. Chem. Soc.* **2005**, *127*, 5689–5694.
43. Kumar, S.; Aaron, J.; Sokolov, K. Directional Conjugation of Antibodies to Nanoparticles for Synthesis of Multiplexed Optical Contrast Agents with Both Delivery and Targeting Moieties. *Nat. Protoc.* **2008**, *3*, 314–320.
44. Qian, X.; Peng, X.-H.; Ansari, D. O.; Yin-Goen, Q.; Chen, G. Z.; Shin, D. M.; Yang, L.; Young, A. N.; Wang, M. D.; Nie, S. In Vivo Tumor Targeting and Spectroscopic Detection with

Surface-Enhanced Raman Nanoparticle Tags. *Nat. Biotechnol.* **2008**, *26*, 83–90.
45. Lin, S.-Y.; Tsai, Y.-T.; Chen, C.-C.; Lin, C.-M.; Chen, C.-h. Two-Step Functionalization of Neutral and Positively Charged Thiols onto Citrate-Stabilized Au Nanoparticles. *J. Phys. Chem. B* **2004**, *108*, 2134–2139.
46. Wang, L.; Shi, X.; Kariuki, N. N.; Schadt, M.; Wang, G. R.; Rendeng, Q.; Choi, J.; Luo, J.; Lu, S.; Zhong, C. J. Array of Molecularly Mediated Thin Film Assemblies of Nanoparticles: Correlation of Vapor Sensing with Interparticle Spatial Properties. *J. Am. Chem. Soc.* **2007**, *129*, 2161–2170.
47. Yokoyama, M.; Okano, T.; Sakurai, Y.; Kikuchi, A.; Ohsako, N.; Nagasaki, Y.; Kataoka, K. Synthesis of Poly(Ethylene Oxide) with Heterobifunctional Reactive Groups at its Terminals by an Anionic Initiator. *Bioconjugate Chem.* **1992**, *3*, 275–276.
48. Akiyama, Y.; Otsuka, H.; Nagasaki, Y.; Kato, M.; Kataoka, K. Selective Synthesis of Heterobifunctional Poly(Ethylene Glycol) Derivatives Containing Both Mercapto and Acetal Terminals. *Bioconjugate Chem.* **2000**, *11*, 947–950.
49. Park, J. E.; Lenter, M. C.; Zimmermann, R. N.; Garin-Chesa, P.; Old, L. J.; Rettig, W. J. Fibroblast Activation Protein, a Dual Specificity Serine Protease Expressed in Reactive Human Tumor Stromal Fibroblasts. *J. Biol. Chem.* **1999**, *274*, 36505–36512.
50. Rettig, W. J.; Garin-Chesa, P.; Healey, J. H.; Su, S. L.; Jaffe, E. A.; Old, L. J. Identification of Endosialin, a Cell Surface Glycoprotein of Vascular Endothelial Cells in Human Cancer. *Proc. Natl. Acad. Sci. U.S.A.* **1992**, *89*, 10832–10836.
51. Scanlan, M. J.; Raj, B. K.; Calvo, B.; Garin-Chesa, P.; Sanz-Moncasi, M. P.; Healey, J. H.; Old, L. J.; Rettig, W. J. Molecular Cloning of Fibroblast Activation Protein Alpha, a Member of the Serine Protease Family Selectively Expressed in Stromal Fibroblasts of Epithelial Cancers. *Proc. Natl. Acad. Sci. U.S.A.* **1994**, *91*, 5657–5661.
52. Scott, A. M.; Wiseman, G.; Welt, S.; Adjei, A.; Lee, F. T.; Hopkins, W.; Divgi, C. R.; Nahson, L. H.; Mitchell, P.; Gansen, D. N.; et al. Phase I Dose-Escalation Study of Sibrotuzumab in Patients with Advanced or Metastatic Fibroblast Activation Protein-Positive Cancer. *Clin. Cancer Res.* **2003**, *9*, 1639–1647.
53. Grabar, K. C.; Freeman, R. G.; Hommer, M. B.; Natan, M. J. Preparation and Characterization of Au Colloid Monolayers. *Anal. Chem.* **1995**, *67*, 735–743.
54. Schneider, G.; Decher, G.; Nerambourg, N.; Praho, R.; Werts, M. H. V.; Blanchard-Desce, M. Distance-Dependent Fluorescence Quenching on Gold Nanoparticles Ensheathed with Layer-by-Layer Assembled Polyelectrolytes. *Nano Lett.* **2006**, *6*, 530–536.
55. Dulkeith, E.; Ringler, M.; Klar, T. A.; Feldmann, J.; Javier, A. M.; Parak, W. J. Gold Nanoparticles Quench Fluorescence by Phase Induced Radiative Rate Suppression. *Nano Lett.* **2005**, *5*, 585–589.
56. Garin-Chesa, P.; Old, L. J.; Rettig, W. J. Cell Surface Glycoprotein of Reactive Stromal Fibroblasts as a Potential Antibody Target in Human Epithelial Cancers. *Proc. Natl. Acad. Sci. U.S.A.* **1990**, *87*, 7235–7239.
57. Welt, S.; Divgi, C. R.; Scott, A. M.; Garin-Chesa, P.; Finn, R. D.; Graham, M.; Carswell, E. A.; Cohen, A.; Larson, S. M.; Old, L. J. Antibody Targeting in Metastatic Colon Cancer: A Phase I Study of Monoclonal Antibody F19 against a Cell-Surface Protein of Reactive Tumor Stromal Fibroblasts. *J. Clin. Oncol.* **1994**, *12*, 1193–1203.
58. Kumar, S.; Kortum, R. R. Optical Molecular Imaging Agents for Cancer Diagnostics and Theraputics. *Nanomedicine* **2006**, *1*, 23–30.
59. El-Sayed, I. H.; Huang, X.; El-Sayed, M. A. Selective Laser Photo-Thermal Therapy of Epithelial Carcinoma Using Anti-EGFR Antibody Conjugated Gold Nanoparticles. *Cancer Lett.* **2006**, *239*, 129–135.
60. Huang, X.; El-Sayed, I. H.; Qian, W.; El-Sayed, M. A. Cancer Cells Assemble and Align Gold Nanorods Conjugated to Antibodies to Produce Highly Enhanced, Sharp, and Polarized Surface Raman Spectra: A Potential Cancer Diagnostic Marker. *Nano Lett.* **2007**, *7*, 1591–1597.
61. Loo, C.; Hirsch, L.; Lee, M.-H.; Chang, E.; West, J.; Halas, N.; Drezek, R. Gold Nanoshell Bioconjugates for Molecular Imaging in Living Cells. *Opt. Lett.* **2005**, *30*, 1012–1014.
62. Durr, N. J.; Larson, T.; Smith, D. K.; Korgel, B. A.; Sokolov, K.; Ben-Yakar, A. Two-Photon Luminescence Imaging of Cancer Cells Using Molecularly Targeted Gold Nanorods. *Nano Lett.* **2007**, *7*, 941–945.
63. Mallidi, S.; Larson, T.; Aaron, J.; Sokolov, K.; Emelianov, S. Molecular Specific Optoacoustic Imaging with Plasmonic Nanoparticles. *Opt. Express* **2007**, *15*, 6583–6588.
64. Rahman, M.; Abd-El-Barr, M.; Mack, V.; Tkaczyk, T.; Sokolov, K.; Richards-Kortum, R.; Descour, M. Optical Imaging of Cervical Pre-Cancers with Structured Illumination: An Integrated Approach. *Gynecol. Oncol.* **2005**, *99*, S112–S115.
65. Grabarek, Z.; Gergely, J. Zero-Length Crosslinking Procedure with the Use of Active Esters. *Anal. Biochem.* **1990**, *185*, 131–135.
66. Hermanson, G. T. *Bioconjugate Techniques*; Academic Press: San Diego, CA, 1995.